

Experimental and numerical study on tensile properties of bolted GFRP joints at high and low temperatures

Congcong Xue ^{a,b}, Min Yu ^{a,*}, Biying Yang ^a, Tan Wang ^a, Mohamed Saafi ^b, Jianqiao Ye ^{b,*}

^a School of Civil Engineering, Wuhan University, Wuhan, Hubei Province, 430072, China.

^b Department of Engineering, Lancaster University, Lancaster, LA1 4YR. UK.

Abstract: This paper presents both experimental and numerical studies on bolted glass fiber reinforced polymer (GFRP) joints subjected to uniaxial tension and different thermal conditions (-20 °C, 20 °C and 60 °C). Laboratory tests are conducted to obtain strength, elastic modulus and deformation of the joints. The numerical model is developed using the discrete element method (DEM) that can predict not only the above properties of the joints, but also the failure modes with detailed meso/micro damages that are in consistent with the observations from the tests. The DEM model is also used in the parametric studies to study the influence of the end distance to bolt/hole diameter ratio and the lap width to bolt/hole diameter ratio on the mechanical properties and failure models of the joints.

Keywords: GFRP laminates and bolted joints, tensile properties, high and low temperatures, DEM

* Corresponding authors: ceyumin@whu.edu.cn (M. Yu); j.ye2@lancaster.ac.uk (J.Ye)

1 Introduction

Fiber reinforced polymer (FRP) is a new high-performance material made of matrix material (such as epoxy resin, polyester resin, etc.) and fiber material (such as glass fiber, carbon fiber, etc.) mixed in a certain proportion and compounded by extrusion, drawing and other processes^[1, 2]. Since the 1970s, FRP has been gradually used as the critical components of building and bridge structures^[3-6]. In recent years, GFRP has been increasingly used in building structures as load-bearing materials. These structures usually use bolted joints to transfer internal load between components, with the advantages of easy assembly, dis-assembly, and maintenance. Pultruded GFRP is an orthotropic elastic-brittle material. The load transfer and failure of a bolted GFRP joint are more complex than those of a steel connection, more than half of the failures of which occur in the connection part^[7, 8]. In addition, with the frequent occurrence of extreme weather around the world, the components used in civil engineering generally exposed to severe environment, resulting in great changes in the ambient temperature. For example, in some African countries, the temperature of structures exposed to the outdoor may experience to temperature exceeding 50 °C, while in some Asia countries, the temperature in winter is also below 0 °C. The ambient temperature inevitably affects the performance of the composites^[9-11]. Previous studies have also showed that the material properties of GFRP, such as microstructure and failure mode^[12], strength, stiffness^[9, 13] and shear behaviour^[14], etc., changed greatly at high and low temperatures. Therefore, it is practically important to study the failure characteristics and mechanical responses of bolted GFRP joints under a full range of service temperature range.

Construction and building materials need to meet the requirements of bearing capacity and deformation under normal service conditions. A number of studies have been carried out on the mechanical properties of composite laminates and bolted joints of different geometry and under different temperature conditions^[15-18]. Abd-El-Naby and Hollaway^[19, 20] conducted a series of tensile tests on single and double bolts, considering mainly the influence of the area of plates, the clamping area of bolts, as well as the influence of end distance to bolt on the strength. Turvey^[21, 22] tested pultruded GFRP materials, bolted joints and sub-structures/full-scale structures subjected to tensile, compressive, bending, buckling and collapse loads. Liu et al^[23] conducted tensile tests on pultrusion GFRP single-lap single-bolt connections for various bolt-diameter to plate-thickness ratio, splice plate configurations and loading directions. P.V. Inbanaathan et al.^[24] carried out tensile and flexural tests on GFRP laminates and bonded joints to obtain the ultimate tensile strength, stress strain curves and the flexural modulus. Yang et al.^[25] presented the mechanical performances of the single-bolted double-lap joints with steel bolts by torque-preload and tensile experiments. The results of these investigations show that the size and shape of components have a significant effect on the test results. In addition, temperature conditions were also considered in some of the reported research. Bai et al.^[26] conducted axial compression experiments on GFRP laminates under elevated temperatures, and compared the failure mode at different temperatures. Cooper and Turvey et al.^[27-29] studied the bearing capacity and deformation of pultruded GFRP single-bolt joints of different lap width to bolt / hole diameter ratios (W/D), end distance to bolt / hole diameter ratios (E/D) when they were under four different test temperatures. Toubia et al.^[30] evaluated the residual strengths and failure mechanisms

of bolted double lap pultruded joints in regions of low-to-moderate heat induced exposure.

The above research studied mainly the failure modes of the joints and the influence of some design factors from experimental observations. In order to have a better understanding of the failure of GFRP joints and take full advantages of GFRP in practical design, further numerical research into the failure mechanism, including the consideration of temperature, is required^[31, 32]. Traditional finite element methods are usually used to predict crack initiation and stress distribution, but due to the inherited limitations of classical continuum mechanics, it is difficult to simulate the process of dynamic damage formation and propagation. The non-homogeneous multiphase structure of GFRP leads to the complexity of component failure. It has been shown that discrete element method has advantages in tracking the failure path and predicting the final failure strength at both meso- and micro-scale^[33, 34].

In this respect, with the help of discrete element method, Maheo et al.^[35] simulated the failure of composites under uniaxial tensile load, Le et al.^[36] simulated the delamination, matrix cracking and fiber fracture of FRP laminates. Thus, using the micro modeling method, DEM can effectively determine initial crack and matrix crack distribution^[37, 38]. To the authors' best knowledge, only a few studies have used DEM to simulate materials of larger scale^[35, 37, 39, 40]. Zha et al.^[41] simulated the failure of metal sandwich plate under uniform pressure with DEM. Yu et al.^[42] first tried to simulate bolted joints by DEM and present a procedure to calibrate the micromechanical parameters of the model subjected to axial tension at room temperature. The research has shown great potential of the DEM model in predicting strength of composite materials and structures and presenting detailed local damage and damage propagation at micro-scale. This paper develops the model further to study the uniaxial tensile mechanical properties of bolted GFRP joints at high and low temperatures. Experimental tests are carried out to calibrate the microscopic mechanical parameters for using the discrete element model at high and low temperatures. Geometric parameters of the bolts considered in the study include end distance to bolt/hole diameter ratio (E/D) and lap width to bolt/hole diameter ratio (W/D). Finally, the failure mechanism of the bolted GFRP joints at different temperatures is studied.

2 Tensile tests at high and low temperatures

In order to study the effect of the normal service temperature on the mechanical properties of bolted GFRP joints, tensile properties of bolted joints with end distance of 25 mm are tested at - 20 °C, 20 °C and 60 °C. The bolts of the joints are torque to 3 N-m, which is sufficient to secure the integrity of the joints and enables to qualify the lower bound load capacity of the joints. The mechanical properties and failure modes of the bolted joints at high and low temperatures are obtained by video measurement system, and the influence of temperatures on the GFRP laminates and the bolted GFRP joints is analyzed.

2.1 Specimen details

The test specimens are EXTREN®500 series pultruded GFRP laminates manufactured by Stronwell, UK. The weight percentages of glass fibers and resin are about 30% and 70%, respectively. The glass fibers in the samples are in the form of unidirectional parallel fiber roving (UPFR) and continuous filament mat (CFM)^[42], which determine the rigidity and ultimate stress along the fiber direction, and the properties of the specimens in

the transverse (perpendicular to the fiber) direction. The type of the matrix resin is polyester. The maximum recommended operating temperature for GFRP pultrusion is 65 °C, as it is about the point the matrix changes phase from solid to flow. Laminates with fiber orientation of 0° and 90° and single bolted joints consisting of two laminates with fiber orientation of 0° are tested in this study. The illustrative diagram and dimension of the GFRP samples are shown in Fig. 1 and Table 1, respectively, and the sample dimensions are based on BS 2782 and the specifications defined in [43].

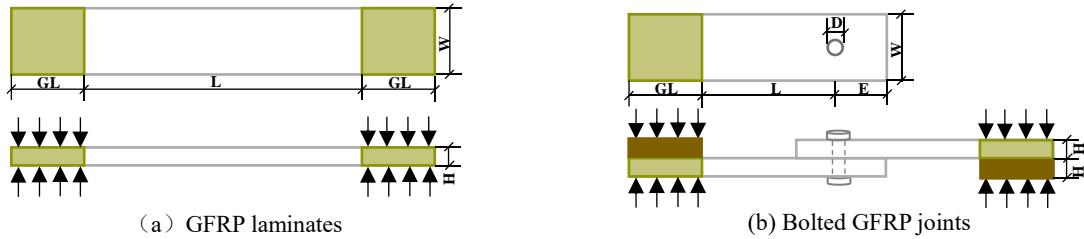


Fig. 1 Illustrative diagram of GFRP laminates and bolted joints

Table 1 Parameters of GFRP laminates and bolted joints

Sample ID	Temperature °C	Length L/mm	Loading zone length GL/mm	Width W/mm	Thickness H/mm	End distance E/mm	Diameter D/mm	Notes
LX-N20	-20	200	50	40	6.4	-	-	
LX-P20	20	200	50	40	6.4	-	-	
LX-P60	60	200	50	40	6.4	-	-	Fig. 1
LY-N20	-20	200	50	40	6.4			(a)
LY-P20	20	200	50	40	6.4			
LY-P60	60	200	50	40	6.4			
JX-N20	-20	100	50	40	6.4	25	10	
JX-P20	20	100	50	40	6.4	25	10	Fig. 1
JX-P60	60	100	50	40	6.4	25	10	(b)

In Table 1, the sample ID in the first column shows the type of the samples and the test temperature. L and J denote, respectively, laminates and bolted joints. X and Y refer to the fiber direction of 0° and 90°. N and P indicate whether the test temperature is Negative or Positive. For example, LX-N20 represents a laminate with fiber orientation of 0° that is tested under an environmental temperature of -20°C.

2.2 Experimental set-up and procedure

As shown in Fig. 2, the electric furnace is used to heat and control the temperature of the specimen. The 30 tons universal testing machine is used to apply loading, and the non-contact video measuring system is used to measure the deformation. The IMETRUM non-contact video gauge (video gauge5.0) has an accuracy of up to 1 μm, which can track more than 100 target points at the same time and perform dynamic real-time analysis with measurement frequency of over 400Hz. The non-contact video measuring system is also used in the previous work [42], where detailed settings for the tests can be found. In this paper a specifically designed arrangement for the lamp belts and mirrors is used to simultaneously measure the deformation on the front and side of the joints to capture their complex 3D deformation. Considering that the video measuring instrument is sensitive to light intensity, two high and low temperature resistant lamp belts are configured to reduce reflection, thus providing

photos of higher quality. A mirror is mounted and positioned in the electric furnace along with the video measuring instrument, such that the deformation and damage of the side surface of a joint can be measured and monitored at the same time when the measurements of the front surface are taken.

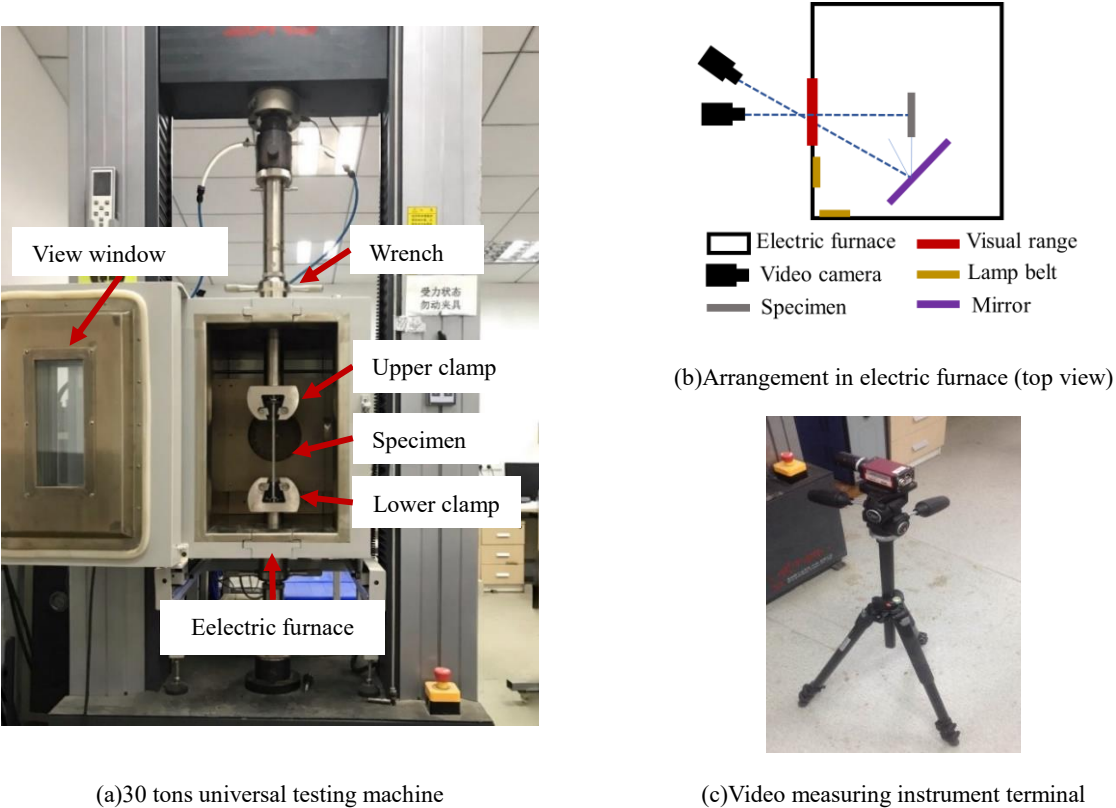


Fig. 2 Schematic diagram of test equipment

The surface of the specimen is pretreated and marked with speckles and lines for strain measurement and identification of measuring points. Two high speed cameras are used, one of which is aimed at the front of the specimen, and the other records the side of the specimen through the reflection of the mirror installed in the furnace as shown in Fig. 2(b). The video measuring system is turned on before the furnace is heated, so that the deformation of the specimen during the stage of rising temperatures can be observed in real time. After the displacement-time curve is stabilized, a tensile load at a rate of 1 mm / min is applied until the specimen fails. During the loading process, the temperature fluctuation is controlled within ± 1 °C. The real time data, including deformation, strain and temperature, are collected by the system ready for further analysis. The images of the damaged specimens are taken after the specimens are cooled down.

2.3 Test results and analysis

2.3.1 Material properties

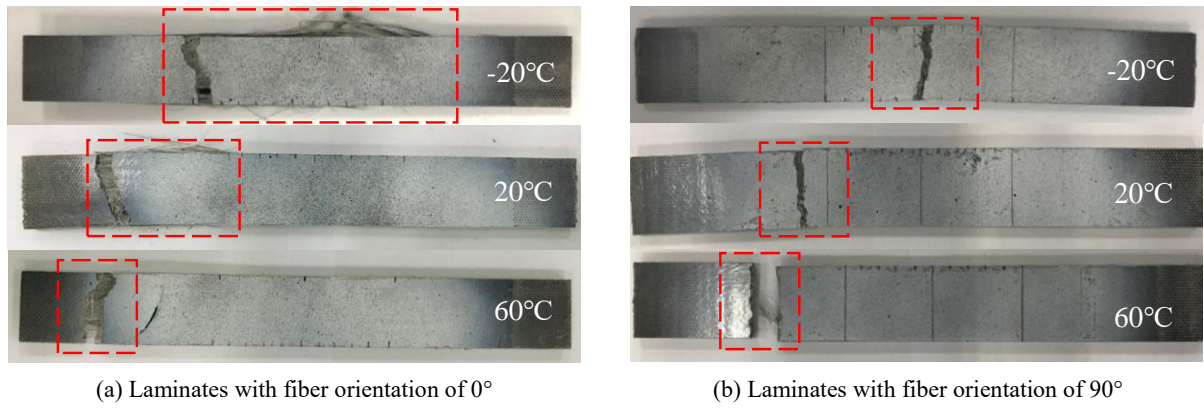


Fig. 3 Failure of GFRP laminates

The tensile failure of the laminates with fiber orientation of 0° at different temperatures is shown in Fig. 3(a). When the temperature is -20°C , the specimen fails brittly. The time from the appearance of visible crack to the final failure of the specimen is very short with obvious fiber bursting. The failure section is close to the middle of the specimen. When the temperature is 20°C , the failure mode of the specimen is still brittle, but exhibits some ductility with only a small amount of fiber bursting. The damaged section is closed to the free edge. When the temperature is 60°C , the failure is more ductile and almost no fiber bursting is observed. The damaged section moves further to the free edge. The failure modes of the laminates with fiber orientation of 90° at different temperatures are not very different (Fig. 3 (b)), which are both tensile failure of cross section. As the temperature rises, the damage location gradually moves from the middle to the free edge of the laminates.

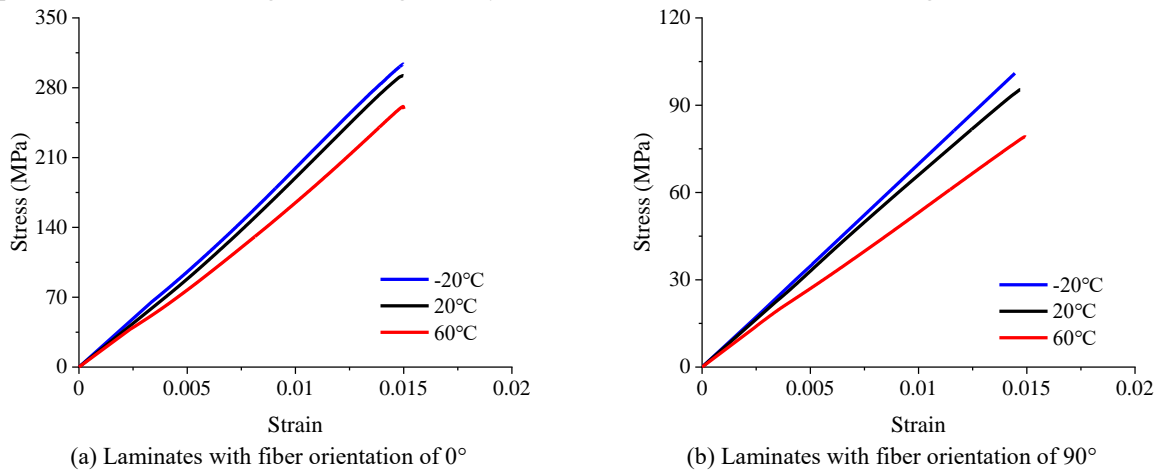


Fig. 4 Stress-strain curves of laminates at different temperatures

The stress-strain curves of the laminates with fiber orientation of 0° at different temperatures are plotted in Fig. 4 (a). The stress is calculated by dividing the bearing capacity with the cross-sectional area of the laminate, and the strain is the elongation divided by the original length between the two measuring points in the tensile direction. It can be seen that the peak stress and elastic modulus decrease with the increase of temperature, and the slope of the curve tends to decrease. The peak stresses of the laminates are 304 MPa, 292 MPa and 261 MPa respectively, when they are at -20°C , 20°C and 60°C , representing an increase of 4% and a decrease of 11% when compared with the peak stress at 20°C . At -20°C and 60°C , the elastic modulus of the laminate increases by +6% and -12%, respectively. The above test results clearly show that temperature increase has a greater effect on the stress of the laminates. Accordingly, the peak stress of the laminates with fiber orientation of 90° at different

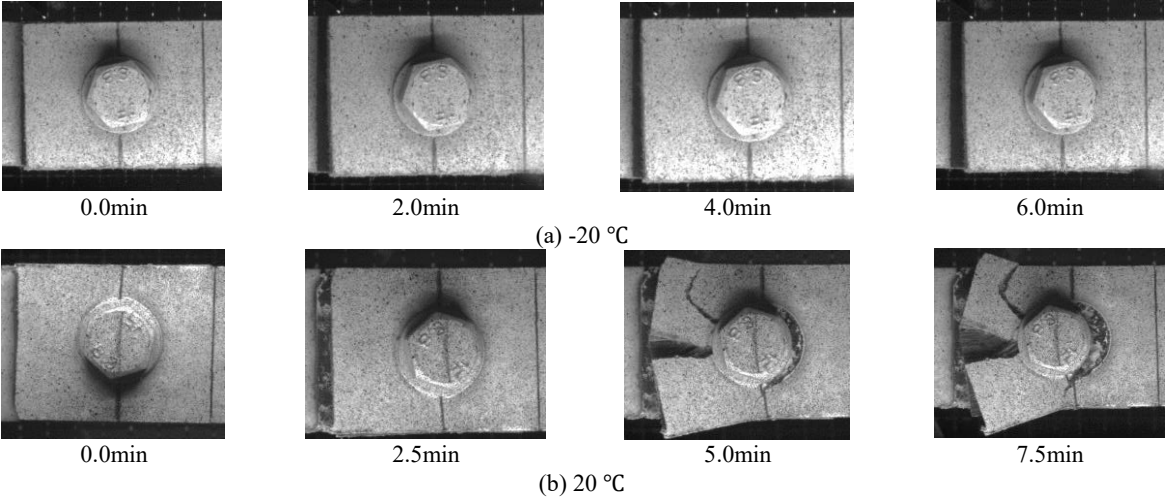
temperatures are 101 MPa, 95 MPa and 79 MPa, respectively (Fig. 4 (b)). Although the direction of the fiber in the laminates in Fig. 4 (a) and (b) is different, the effects of temperature on the peak stress and elastic modulus are consistent.

2.3.2 Failure mode and damage evolution of bolted joints



Fig. 5 Failure modes of bolted joints at high and low temperatures

At -20°C, 20°C and 60°C, the bolted joints show three different failure modes, namely delamination failure, splitting failure and shear failure, as shown in Fig. 5. When the temperature is -20 °C, the specimen is brittle, and there are almost no visible cracks on the front of the laminates, while the delamination caused by the crack in the laminates can be seen from the side view. The dislocation between the two laminates and the rotation of the bolt are relatively small. It is speculated that the stresses are transformed between layers by the resin, which fails before the longitudinal force reaches the ultimate stress, resulting in delamination of the laminates. When the temperature is 20 °C, the failure mode is mainly splitting. The cracks develop from the periphery of the hole. As the load increases, the cracks finally penetrate to the free edge, and the fiber is torn along the longitudinal direction of the laminates. When the temperature is 60 °C, as the loading proceeds, the bolt extrudes the overlapping part towards the free edge forming two through cracks, so the failure mode is shear failure. There is no obvious fiber bursting on both sides, the shear surface is relatively flat, and the fibers around the shear crack are directly staggered to produce a large displacement. Net-section failure of the joints mainly occurs at 20 °C and 60°C. Compared with 20 °C, the damage range of 60 °C is smaller, indicating that the laminate is weakened at high temperature, but still has not yet reached the transformation temperature of GFRP.



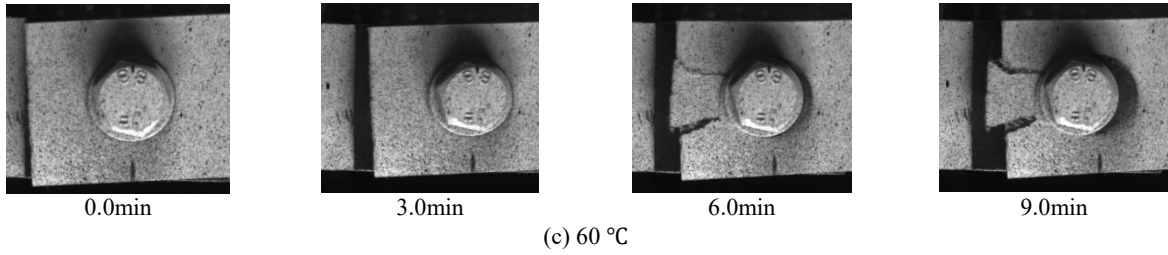


Fig. 6 Frontal failure processes of bolted joints at high and low temperatures

In order to study the failure mechanism of the bolted joints at different temperatures, the non-contact video measuring instrument introduced in the last section was again used to record the damage evolution of the front and the side surface of the joints at different temperatures, as shown in Fig. 6 and Fig. 7 respectively.

Fig. 6 shows the front view of the failure process of the joints at the three temperatures. At -20°C , the front face of the bolted joint does not show any visible damage. At 20°C , as the load increases, sliding displacement occurs between the two plates. This is followed by a single middle crack occurring from the free edge of plate to the bolt. A large stress concentration tends to occur in the longitudinal direction of the laminates, which also accelerates the damage around the hole, such as the widening of the cracks and gradual bursting and dispersion of the fibers. At 60°C , with the increase of load, visible deformation of the two laminates, which is followed by bearing damage at the bolt-laminate contact, pushing the circle of the hole to form an elliptical shape and eventually cause shear out failure. Two cracks are formed on both sides of the bolt.

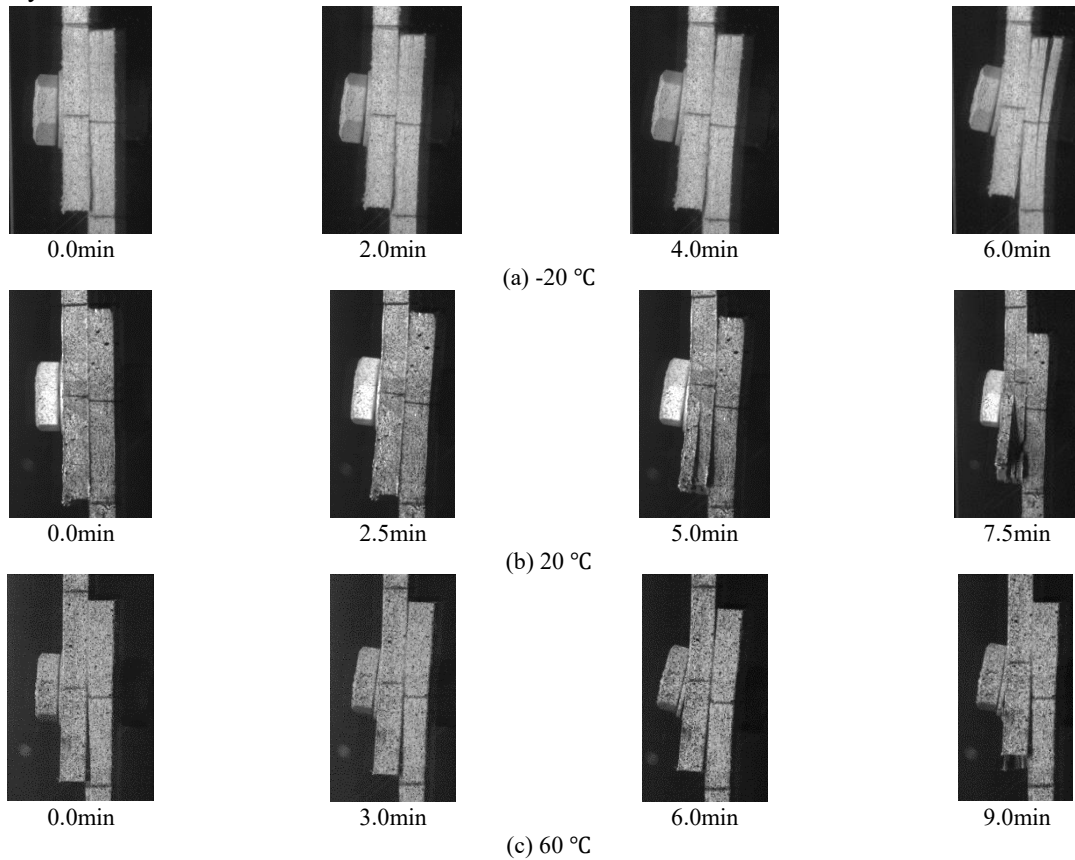


Fig. 7 Lateral failure processes of bolted joints at high and low temperatures

The side views of the failure processes of the joints at the three temperatures are compared in Fig. 7. It is not difficult to see that the bolts rotate with the increase of the load. The rotation angles of the bolts at failure are

between 11° and 16°, so there is only a small difference in the degree of rotation at the three temperatures. When the components fail, significant delamination occurs on the sides at -20°C and 20°C, warpage occurs at -20°C, while the laminates at other temperatures remain relatively tight and flat.

2.3.3 Strength and deformation

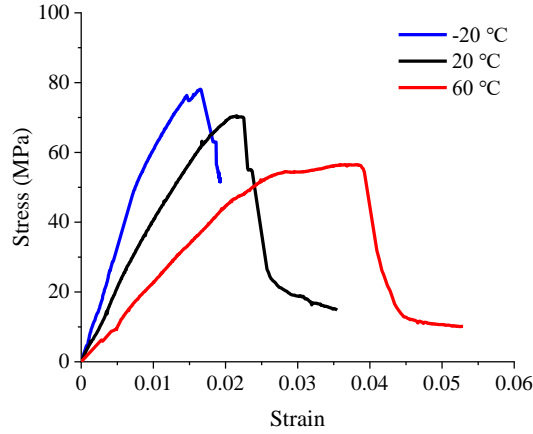


Fig. 8 Stress-strain curves of bolted joints at different temperatures

The stress-strain curves of the bolted joints at the three temperatures are drawn in Fig. 8. With the increase of temperature, the peak stress and elastic modulus of the bolted joints decrease, the displacement at failure increases. At -20, 20 and 60°C, the peak stresses of the bolted joints are 78.1 MPa, 70.5 MPa and 56.5 MPa, respectively. The peak stress at -20°C is 11% higher than that at 20°C, with a lower ductility. At 60 °C, the peak stress of the bolted joint is 20% lower than that at 20°C, but with a much higher ductility. The peak strains before failure are 0.016, 0.022 and 0.038 respectively. Compared with 20°C, the peak strain at -20°C and 60°C are increased by -24% and +76%, respectively. The elastic modulus at -20°C and 60°C increased by +52% and -47% respectively compared with normal temperature.

Under the three temperatures, the cracks of the bolted joints start from different positions around the hole and develop along different paths, producing three different failure modes, namely delamination failure, splitting failure and shear failure, which shows that temperature has a great influence on the failure mode of the bolted joints. This also means that the tensile failure mechanism of the bolted joints subjected to different temperatures is also different. Comparing the tensile properties of the bolted joints at -20°C and 60°C to those at 20 °C, it appears that the properties of the bolted joints are more sensitive to a temperature increase.

As the temperature increases, the reinforcing effect of the fibers in the material decreases gradually, and the elastic modulus and peak stress also decrease. The strain of the laminates at failure is minimal at a lower temperature, and increases with the increase of temperature. This is because with the increase of temperature, the matrix material of the laminate becomes softer and the fracture strain increases, resulting in an increase in the overall strain of the bolted joints. While at a lower temperature, the matrix material becomes more brittle and the overall fracture strain decreases, resulting in a reduction in the strain of the bolted joints.

The above test results will be used in the following section to calibrate the micro parameter for the discrete element numerical model.

3 Discrete element simulation at high and low temperatures

3.1 Discrete element model

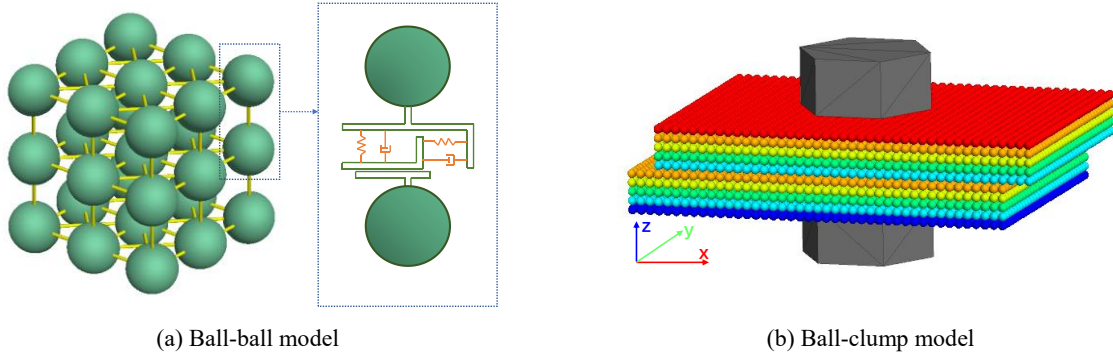


Fig. 9 3D model of the bolted joints

Discrete element model is composed of a finite number of rigid particles. The arrangement of particles has a greater influence on the simulation results, and the regular arrangement can be simulated at the component level compared with the irregular arrangement. Wan et al.^[38] concluded that the extended two-dimensional hexagons and squares have better simulation results for composite laminates. Therefore, the laminate model in this paper selects a regular square arrangement, with particles arranged orthogonally and of the same size. The fiber and matrix are homogenized with anisotropy properties, as shown in Fig. 9(a). The contacts between particles are the linear parallel-bond, which can transmit both force and moment across the interfaces. The damping coefficient of the model is set to be 0.5 to approximate the quasi-static conditions. The bolted joint to be modelled is composed of two laminated plates that are jointed together with a metal bolt of diameter 10mm, as shown in Fig. 9(b).

Table 2 Particle size was taken according to width and thickness of bolt joint model

Direction	Size/mm	Number of model particles		Model dimension (mm)	Error/%
		Calculated	Rounded down		
Width direction	L: 100	80	80	100	0
	W: 40	32	32	40	0
	H: 6.4	5.12	5	6.25	-2.34
	E/D: 2.5	2	2	2.5	0
	D along the length: 10	8	8	10	0
	D along the width: 10	8	8	10	0
	W-D: 30	24	24	30	0
Thickness direction	L: 100	78.125	78	99.84	-0.16
	W: 40	31.25	31	39.68	-0.8
	H: 6.4	5	5	6.4	0
	E/D: 2.5	1.953	1	1.28	-48.8
	D along the length: 10	7.813	7	8.96	-10.4
	D along the width: 10	7.813	7	8.96	-10.4
	W-D: 30	23.438	23	29.44	-1.87

In order to reduce the complexity of the model, the small tightness generated by the bolt is ignored. The bonds between the two laminates and between the plates and the bolt are simulated by the ball-to-ball and the ball-clump model^[44], respectively, as shown in Fig. 9. The particle size of the laminates can be defined by either

the ratio of the width of the model to the number of particles across the width, or the ratio of the thickness of the model to the number of particles across the thickness, such that one of the ratios is an integer and the other is as close to an integer as possible. If one of the ratios is not an integer, the size of the model may be slightly smaller than the actual size of the sample, representing an approximate and conservative model of the sample. Table 2 shows that the size of the model when the width direction and the thickness direction are, respectively, exactly divided by the number of particles and the associated errors in the size of other directions. It can be seen that when the diameter is 1.25mm, the width direction is exactly divided by the number of particles while thickness of the model is 2.34% thinner than that of the sample. This causes a small error in the bearing capacity of the model, which was rectified by multiplying the stress at failure with the actual cross section area of sample. 1.25mm is selected as the diameter of the particles in the following simulation.

3.2 Calibration of the model at high and low temperatures

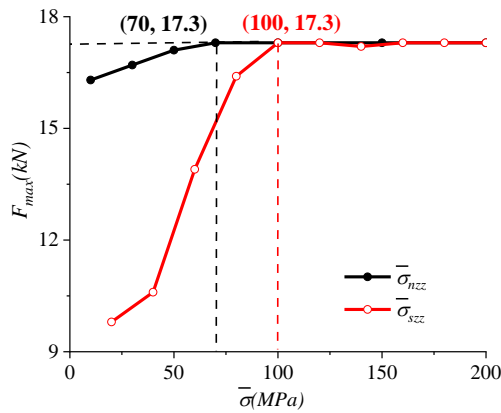


Fig. 10 Calibration of $\bar{\sigma}_{nzz}$ and $\bar{\sigma}_{szz}$ of 20 °C

The strength parameters in the through-thickness (Z) direction of the model can be calibrated by the test results. The bond strength in the Z direction has two components, i.e, the normal strength ($\bar{\sigma}_{nzz}$) and the tangential strength ($\bar{\sigma}_{szz}$). $\bar{\sigma}_{nzz}$ plays a key role in the delamination in the Z direction, while $\bar{\sigma}_{szz}$ mainly improves the shear resistance of the laminate. In order to investigate the effects of these two strengths on the tensile failure mode and bearing capacity of the bolted joints at 20 °C, the control variable method is used in the simulations. A large value of $\bar{\sigma}_{szz}$ is taken first with variable $\bar{\sigma}_{nzz}$. At 20 °C, the predicted tensile force at failure is then compared with the test results in Fig. 8, as shown in Fig. 10. It can be seen from the figure that when $\bar{\sigma}_{nzz}$ is 70MPa, the predicted tensile force is almost equal to the failure forced from the test (Fig. 8). Similarly, by fixing $\bar{\sigma}_{nzz}$, it is found that from Fig. 10 that when $\bar{\sigma}_{szz} = 100$ MPa, the tensile force at failure is consistent with the test results. Similarly, the $\bar{\sigma}_{nzz}$ and $\bar{\sigma}_{szz}$ at -20 °C and 60 °C can be calibrated. Since the material of the laminate is transversely isotropic, $\bar{\sigma}_{nyy}$ is equal to $\bar{\sigma}_{nzz}$. It is found that the change of the tangential strength, $\bar{\sigma}_{sxx}$ and $\bar{\sigma}_{syy}$, have little effect on the bearing capacity and failure model of tensile plate, therefore, $\bar{\sigma}_{sxx}$ and $\bar{\sigma}_{syy}$ are set to a large value to avoid any premature failure. The normal strength of the bond, i.e., $\bar{\sigma}_{nxx}$ in the longitudinal (X) direction and $\bar{\sigma}_{nyy}$ in the width (Y) directions at different temperatures can be obtained by comparing the results from the model and the tests of laminates, respectively, by applying tensile load in the fiber direction. Table 3 shows the calibrated bond strength at different temperatures.

Table 3 The bond strength in each direction at high and low temperatures (MPa)

Direction	Stress	-20 °C	20 °C	60 °C
XX	$\bar{\sigma}_{nxx}$	340	330	280
	$\bar{\sigma}_{sxx}$	100e2	100e2	100e2
YY	$\bar{\sigma}_{nyy}$	80	70	45
	$\bar{\sigma}_{syy}$	100e2	100e2	100e2
XY	$\bar{\sigma}_{nxy}$	150	50	30
	$\bar{\sigma}_{sxy}$	100e2	100e2	100e2
ZZ	$\bar{\sigma}_{nzz}$	80	70	45
	$\bar{\sigma}_{szz}$	150	100	80

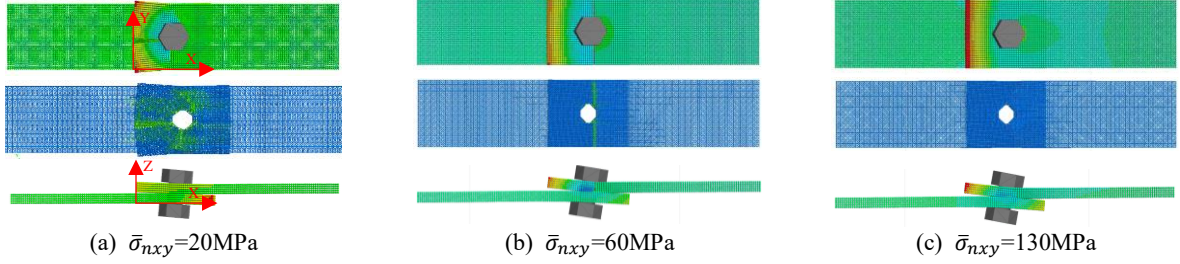


Fig. 11 Effect of $\bar{\sigma}_{nxy}$ on failure mode of bolted joints at 20 °C

The failure mode of the bolted joints at 20 °C in Fig. 11 shows that $\bar{\sigma}_{nxy}$ has an important impact on the failure mode of the bolted joints. When $\bar{\sigma}_{nxy} = 20$ MPa, the failure mode of the bolted joints is splitting failure (Fig. 11 (a)). With the increase of $\bar{\sigma}_{nxy}$, the ratio of $\bar{\sigma}_{nxx}$ and $\bar{\sigma}_{nxy}$ decreases, and the failure mode changes from splitting failure to tensile failure (Fig. 11 (b)). As $\bar{\sigma}_{nxy}$ continues to increase, the load capacity of the bolted joints increases but at a significantly reduced rate. When $\bar{\sigma}_{nxy}$ increases to a value that fails the bond only in the Z direction of the laminates, the failure mode changes from tensile failure to delamination failure in the Z direction (Fig. 11 (c)). To sum up, the failure mode and ultimate peak stress of the bolted joints are different with different $\bar{\sigma}_{nxy}$, which suggests that if the failure mode and peak stress of the bolted joints are known, $\bar{\sigma}_{nxy}$ can be determined by comparing the peak stress (Fig. 8) and failure mode from the bolted joint tensile tests and the simulation results.

3.3 Comparison between simulation and test results

After the above parametric calibration, the bolt joint is modelled by the DEM at different temperatures. The simulation results are compared with the experimental results.

3.3.1 Comparison of failure models

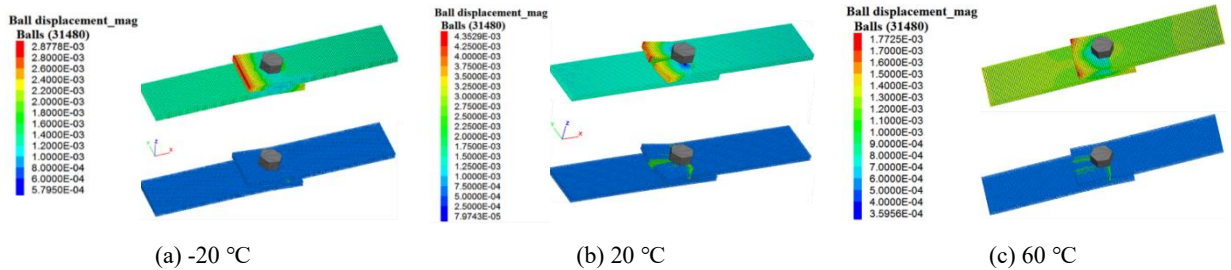


Fig. 12 Failure modes at different temperatures

The simulated failure modes at different temperatures are shown in Fig. 12, which is consistent with the failure modes observed from the experiment. The top is the particle diagram, which presents the particle

displacement, and the bottom is the bond diagram after hiding the particle, where the green and blue bonds represent the broken and unbroken bonds, respectively. The failure mode at the $-20\text{ }^{\circ}\text{C}$ is delamination since no obvious through cracks are observed on the surface of the laminates. At $20\text{ }^{\circ}\text{C}$, the laminate fails due to splitting, and the longitudinal crack runs through the hole to the free edge of the overlap region. Transverse cracks originating from the bolt-hole are also predicted near the location where the cross section of the laminate is smallest. The deformation of the overlap part of the laminate is significant, but the deformation of the non-overlap part is not obvious. At the $60\text{ }^{\circ}\text{C}$, the failure is due to shearing, illustrated by the predicted shear out failure at the end of the overlap region. Similar transverse cracks to those predicted in the room temperature model are also shown across the bolt-hole. The load capacity of the joints predicted by the model decreases with the increase of temperature.

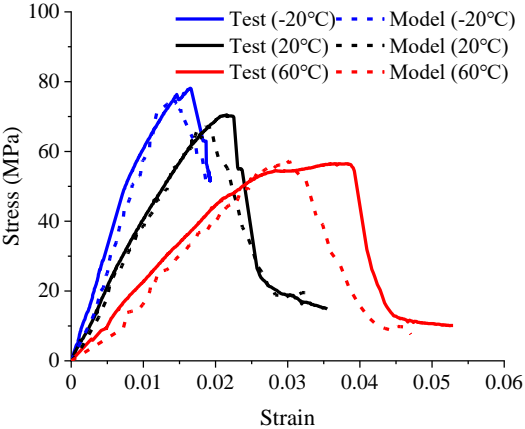
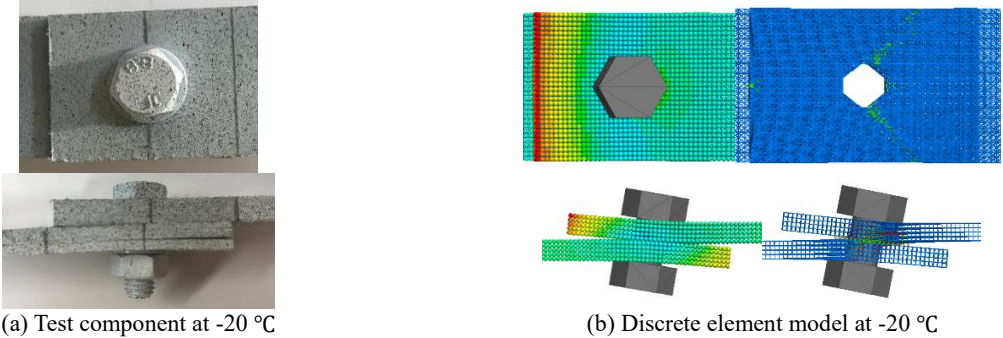


Fig. 13 Stress-strain curves of bolted joints at different temperatures

Fig. 13 compares the predicted stress-strain curves of the bolted joints at different temperatures with those obtained from the experiments. At $-20\text{ }^{\circ}\text{C}$, $20\text{ }^{\circ}\text{C}$ and $60\text{ }^{\circ}\text{C}$, the difference between the peak stress from the numerical simulation and the tests is 3.2%, 4.5% and 1.5%, respectively, with good agreement of the ascending branches of the curves. In general, the model predicts smaller peak stress, especially when the temperature is higher, which is attributed mainly to the linear contact law for the bonds between particles, thus the softening of the matrix material is not considered.

3.3.2 Failure mechanism



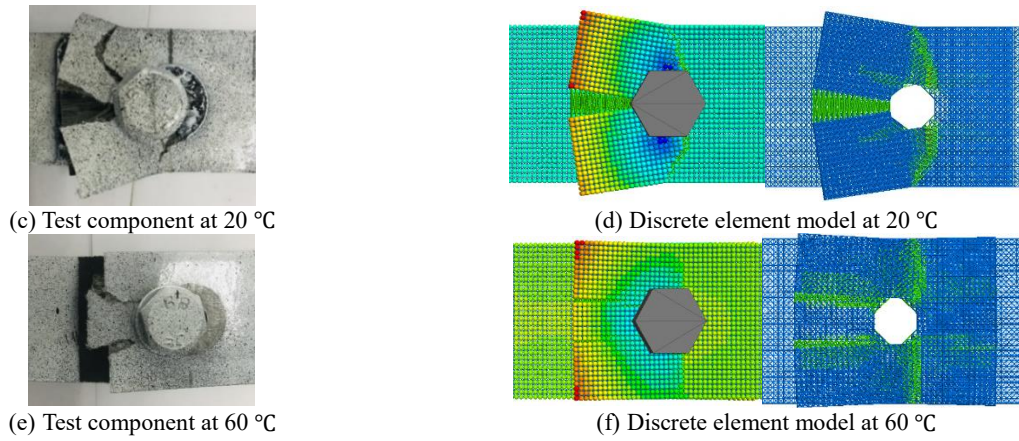
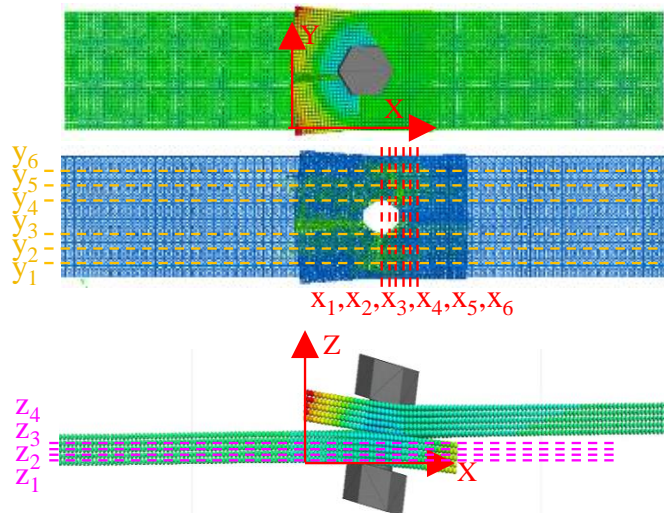


Fig. 14 Comparison of failure diagrams of test components and models at different temperatures

The failure characteristics of the damage shown in Fig. 14 demonstrate good comparisons between the test and the simulation results. Fig. 14 (a), (c) and (e) are photos showing damage of the test specimens after failure, and Fig. 14 (b), (d) and (f) are, respectively, the simulation results where the particle formation (left) and the bond between particles (right) are presented separately to visual the deformation and cracks at failure. The bolt is removed from the diagrams on the right to expose the hidden cracks. On the front face of the joint at -20°C (Fig. 14 (a) and (b)), there are no visible cracks from both the test and the simulation. The simulation results, however, show some fine tensile cracks (broken bond in green) around the hole. The side view of the model in Fig.14(b) shows shear cracks denoted by the broken bonds marked in red, which causes delamination of the laminates. Overall, the simulation results show larger bolt rotation and more cracks than those observed from the test, thus, offer slightly more conservative predictions. Compare with the joint at -20°C , the failure characteristics of the joints at 20°C and 60°C are obviously different, including the initiation, development and final patterns of the cracks (Fig. 14 (c) ~ (f)). It is clear from the figures that the several major cracks radiate from the hole, and there are always transverse cracks running through the laminates (Fig. 14 (d) and (f)). At 20°C , three main cracks are formed around the hole, one of which runs to the transverse edge causing the final failure. At 60°C , four main cracks occur around the hole, and the two longitudinal cracks penetrate to the edge due to shear failure.



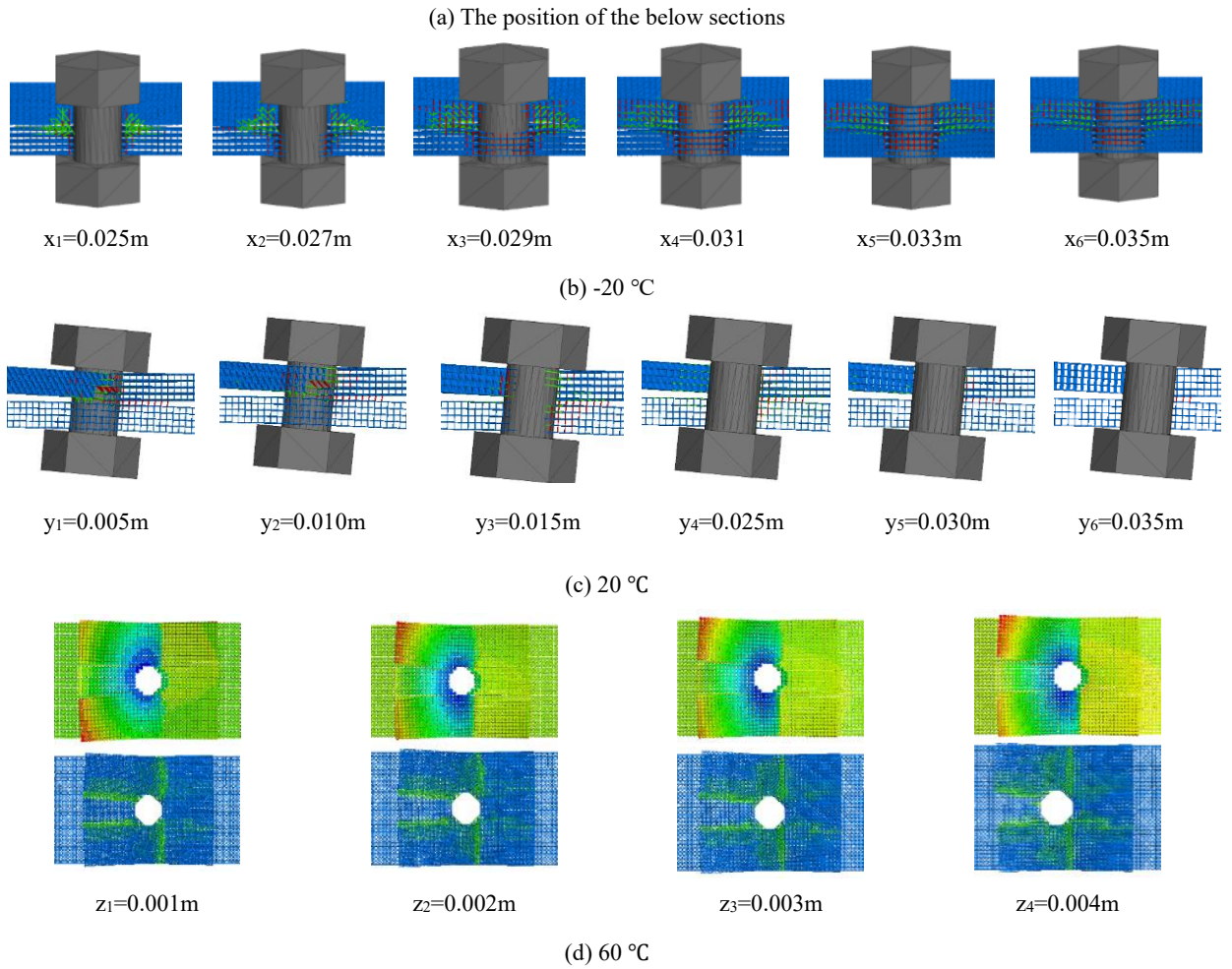


Fig. 15 Development of the cracks in components at different temperatures

To study further the failure mechanism of the bolted joints at different temperatures, sections of the model are taken to observe the internal damage as shown in Fig.15. Six cross-sections are taken, respectively, in the X and Y directions to show the bonds when the joints are under -20 °C and 20. For the model at 60 °C, four cross-sections are taken in the Z direction to show both the particle formation and the bonds. The positions of the sections are shown in Fig. 15(a). In Fig. 15, tensile and shear failure of the bonds are denoted by green and red, respectively.

It can be seen from Fig. 15 (b) that the closer to the hole, the more likely the bonds are to fracture to form cracks at -20 °C. And through cracks (red bonds) in the XY plane ($x = 0.108\text{m}, 0.110\text{m}$) have clearly occurred within the laminate. At 20 °C (Fig. 15(c)), the internal damage in the XY plane is few, mainly concentrated around the hole, and the damage of each section also changes little in the Y direction, indicating that the bolted joint at 20 °C mainly occurs splitting failure. At 60 °C, the relative displacement of each layer within the plate is not significant (Fig. 12(c)). However, the closer to the contact surface of the two plates, the wider the fracture range of the bond is (Fig. 15 (d)). The diffuse nature of the bond damage at $z = 0.004\text{m}$ suggests that the cracks start from the hole of the plate and gradually transfer to the outer side of the plate. And the cracks are through in the thickness direction. Although the visible cracks in the test are shear and tensile cracks, in fact, the damage is also very serious inside the plate.

In practical tests, the failure laws and processes of bolted joints cannot be visualized intuitively. Instead,

with the help of discrete element model, the failure processes and mechanism can be accurately simulated and revealed.

4 The impact of geometric design on the failure of bolted joints

Several experimental studies have shown that E/D and W/D of a bolted joint have a great impact on the failure of the joint^[22, 29, 38, 45]. Therefore, in this section, the calibrated discrete element model is used to simulate and analyze a set of bolted joints with different E/D (2,2.5,3,4,5) and W/D (3,4,5,6) at different temperatures.

4.1 The influence of E/D

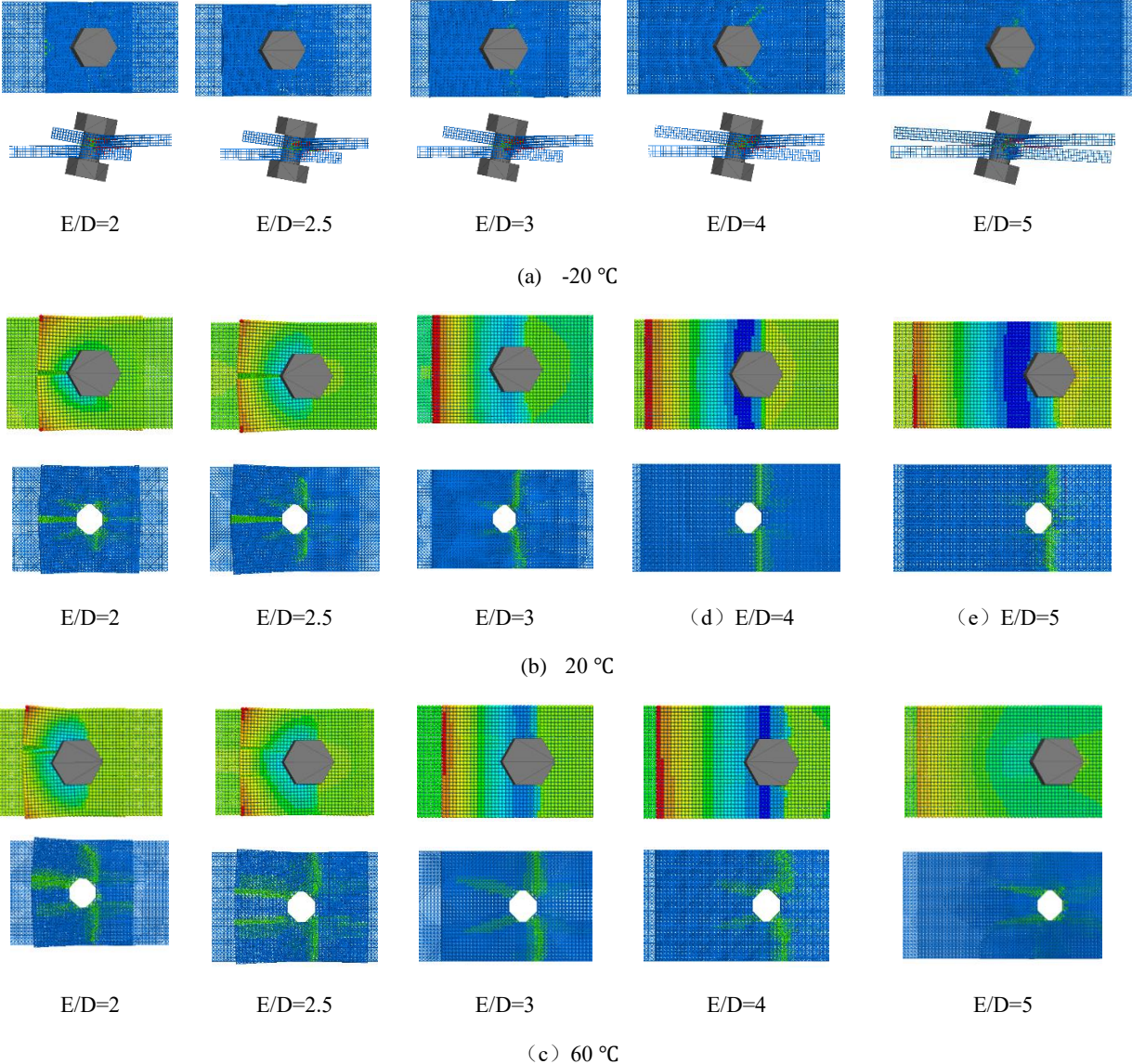
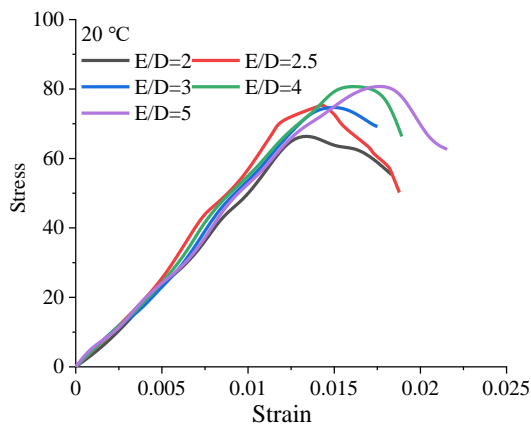


Fig. 16 Failure modes of bolt joints with different E/D

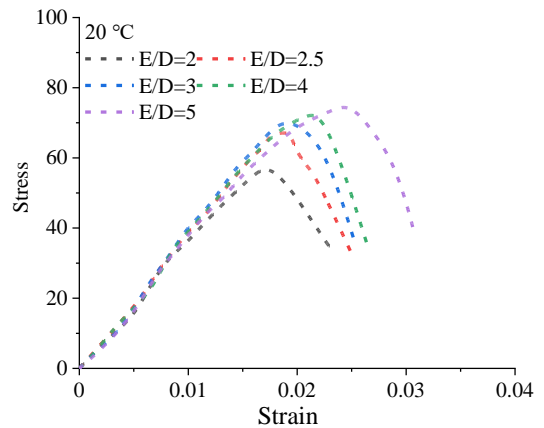
The simulation results of tensile failure of the bolted joints at different temperatures are shown in Fig. 16. At -20 °C, the simulations show delamination failure (Fig. 16 (a)) for all the E/D considered here. However, when $E/D \geq 3$, transverse cracks begin to appear around the hole and become more and more obvious with the increase of E/D. The results also show that no cracks through the cross section are formed before delamination failure occurs. Compared with the side view of bolted joints, it can be seen that E/D has little effect on the rotation of bolts.

At 20 °C (Fig. 16 (b)), when E/D is less than 3, the bolted joints fail due to splitting. When $E/D = 2$, radial cracks are formed around the hole, but the main crack is the one leading to the free edge; When $E/D = 2.5$, the transverse crack develops rapidly. Due to the early formation of the longitudinal crack leading to the free edge, the overall failure mode of the bolted joints is still splitting failure. When $E/D \geq 3$, there fewer radial cracks around the hole, and the fracture energy is mainly dissipated through the transverse crack across the width of the laminate, thus the failure mode changes to tensile failure. Therefore, as E/D increases, the crack causing failure changes from the longitudinal to transverse crack, and the failure mode changes from splitting to tensile.

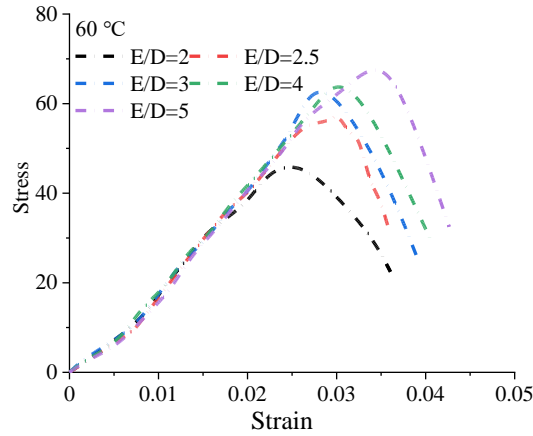
At 60 °C, when $E/D = 2$ and 2.5, the bolted joints fail due to shear (Fig. 16 (c)). The particle diagram shows a longitudinal crack from the bolt to the free edge, which is not a typical characteristic of shear failure. However, the bond diagram shows a second longitudinal and almost parallel crack that has not yet penetrated to the free edge. This suggests that the two longitudinal cracks are formed simultaneously due to the shear stresses generated by the force acting on the bolt-laminate contact. With the increase of E/D , the lap length increases, and the failure mode changes to tensile failure. The particle diagram shows that the particle displacement of the lap section varies linearly along the X direction. When $E/D = 5$, the bond diagram shows that the damage of the laminate is mainly concentrated at the position where the bolt and the laminate are squeezed, and the crack does not penetrate to the free edge, so it can be judged that the failure mode is pressure failure. In contrast to the failure mode at normal temperature, shear failure and pressure failure appear at 60 °C, depending on the strength of the normal bond in the XY and YY direction, respectively. In terms of crack development, this may be due to the fact that the high temperature reduces the strength of the normal bonds in the XY and YY direction more than that in the XX direction.



(a)



(b)



(c)

Fig. 17 Stress-strain curves of bolted joints at different temperatures vs E/D

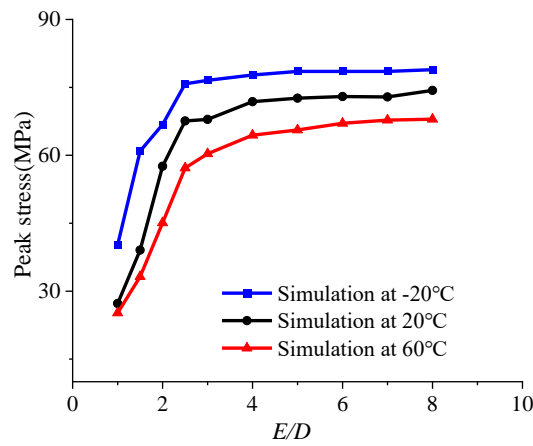


Fig. 18 Relationship between the peak stress and different E/D at different temperatures

From the stress-strain curves of the bolted joints at different temperatures (Fig. 17) and the relationship between the peak stress and E/D (Fig. 18), it can be seen that with the increase of E/D, the peak stress and the peak strain increase. However, when E/D exceeds 3, the increase rate of the peak stress decreases. The peak stress decreases with the increase of temperature, and the ductility at 60 °C is much greater than that at -20 °C and 20 °C. For a given temperature, the stiffness of the joints with different E/D are virtually the same in the loading stage before the maximum is reached, and are also not much different after the peak stress at 20 °C and 60 °C except E/D=2. Therefore, it can be concluded that E/D has little effect on the elasticity and ductility of the bolted joints.

Table 4 Comparison of failure modes of bolted joints at different temperatures

Temperature	E/D	Failure mode of tests in this paper	Failure mode of tests ^[29]	Failure mode of models
-20 °C	2.5	Delamination failure	--	Delamination failure
	2	Splitting failure	Splitting failure	Splitting failure
20 °C	2.5	Splitting failure	Splitting failure	Splitting failure
	3	Splitting failure	Mainly splitting failure, partial tensile failure	Tensile failure
	4	Tensile failure	Tensile failure	Tensile failure

	5	Tensile failure	Tensile failure	Tensile failure
	2	--	Mainly shear failure, splitting failure also presents	Shear failure
	2.5	Shear failure	Mainly shear failure, splitting failure also presents	Shear failure
60 °C	3	--	Mainly splitting failure, tensile and pressure failure also present	Tensile failure
	4	--	Mainly pressure failure, tensile and splitting failure also present	Tensile failure
	5	--	Mainly pressure failure, tensile failure also presents	Pressure failure

Table 4 shows comparisons of the failure modes predicted by the DEM model and the test results of Turvey and Szulik [29] and this paper. At 20 °C, when $E/D < 3$ and $E/D > 3$, the failure modes are splitting failure and tensile failure, respectively, the same as those observation from tests. When $E/D = 3$, the tests results showed both splitting and tensile failure among the tested samples. The simulation results show tensile failure with cracks developing in the longitudinal direction towards the free edge. The failure modes of the joints at 60 °C are less comparable between the test and the simulation results. However, the DEM model can simulate at least one of the failure modes, in most of the cases the dominating failure modes, with also predicted crack patterns related to other observed failure modes. Overall, the model can satisfactorily simulate most of the failure modes observed from the tests, though some failure modes are missing. It is believed that the missing modes are associated with some uncertain factors, such as initial defects, temperature fluctuation and operational errors of the tests, etc.

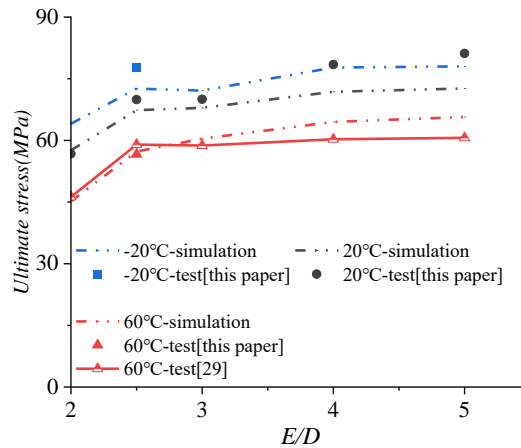


Fig. 19 Ultimate stress vs E/D

Fig. 19 shows the ultimate stresses of the joints with different E/D, where comparisons are made between the simulation results and the test results available in the literature and from this paper. It can be seen that the simulation results are generally agree well with the test results. For all the temperatures considered, the load capacities from simulation are slightly lower than those from the tests, thus provide conservative predictions to the failure loads. It can also be seen from Fig.19 that any increase of the edge distance of the plate, E, does not increase the load capacity significantly after E/D reaches 2.5, especially when the temperature is higher. This is confirmed by the failure modes shown in Fig. 16 where the failure of the joints is likely to be transverse cracking when E/D is greater than 2.5, while end splitting is more likely when E/D is smaller than 2.5.

4.2 The influence of W/D

From the test and simulation results of the bolted joints with different E/D (Fig. 19), E/D has little impact on the peak stress of the joints when it is greater than 2.5. Therefore, the parameter analysis of the impact of W/D is carried out for the joints with E/D of 3.

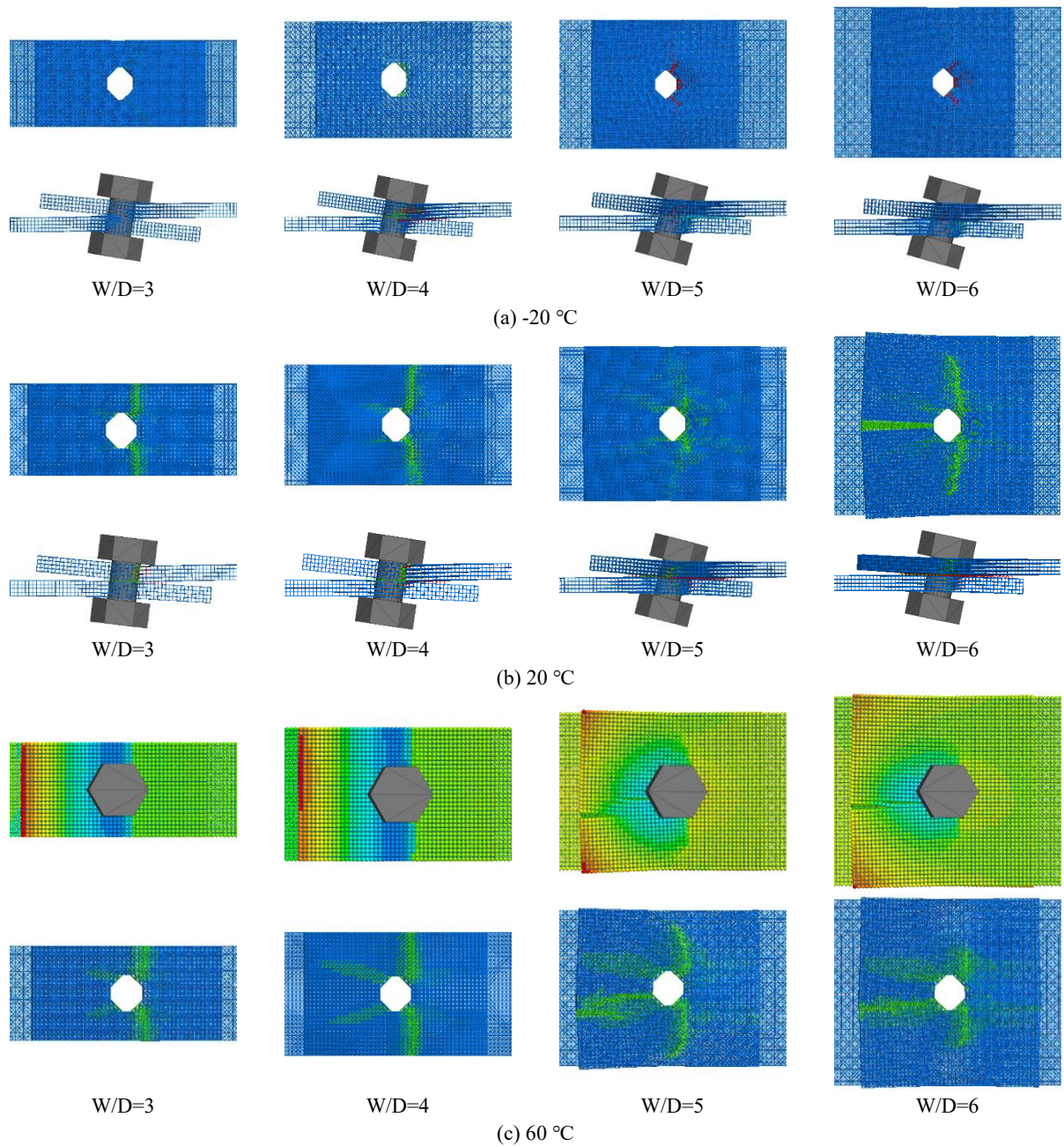


Fig. 20 Failure modes of models with different W/D at different temperatures

Fig. 20 shows discrete element simulation of the joints at different temperatures. At $-20\text{ }^{\circ}\text{C}$ when W/D is 3 and 4, the bolted joints show delamination failure, and there are no visible cracks on the surface of the plates. When W/D increases to 5 or 6, there are still some interior cracks, and damage caused by bolt extrusion appears near the pressed surface of the hole. This indicates that when W/D increases, the failure of bolted joints changes from delamination failure to pressure failure at a low temperature. At $20\text{ }^{\circ}\text{C}$ and $60\text{ }^{\circ}\text{C}$, when $W/D < 5$, the bolted joints are failed by tension; When $W/D = 5$, pressure failure occurs at $20\text{ }^{\circ}\text{C}$. At $60\text{ }^{\circ}\text{C}$, tensile and shear failure coexist. When $W/D > 5$, the bolted joints fail due to end splitting and shear failure, respectively, at $20\text{ }^{\circ}\text{C}$ and

60 °C.

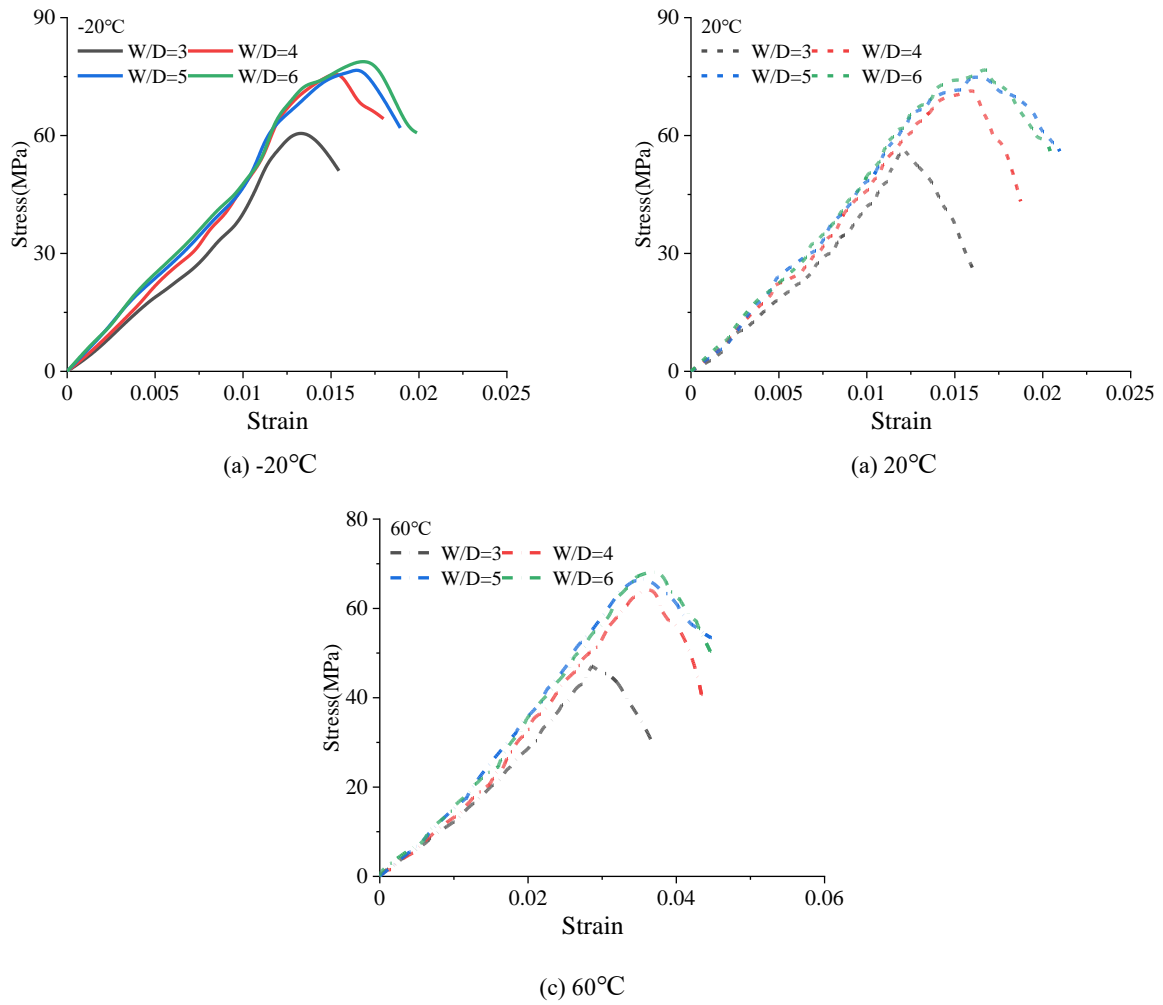


Fig. 21 Stress-strain curves of bolted joints at different temperatures vs W/D

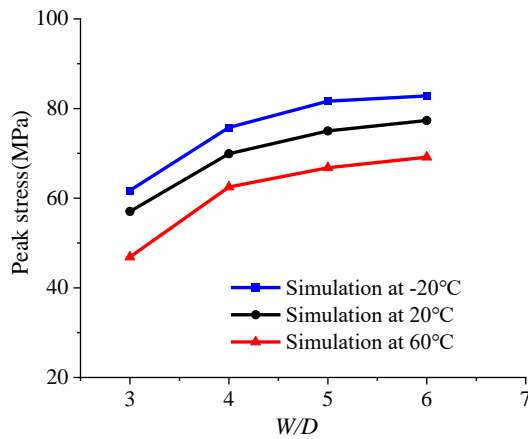


Fig. 22 Relationship between the peak stress and different W/D at different temperatures

Fig. 21 and Fig. 22 show the stress-strain relations and the peak stress of the bolted joints at different temperatures. With the increase of W/D, the peak stress increases gradually. The peak stress increases more quickly When W/D is smaller than 4. Fig. 21 shows that stiffness of the joints is almost the same for the W/D before their respective peak stress is reached, while the slop of the descending branches of the curves only shows good consistency at 60 °C. The main reason for this observation is attributed to the fact that the influence of W/D

on the failure mode at 60 °C is not as great as that at the lower temperatures.

5 Conclusions

In this paper, tensile properties of bolted GFRP joints at high and low temperatures are tested and modeled by the discrete element method that can simulate damage of the material at meso/micro scale. The main work and conclusions are as follows:

(1) The tensile tests of the bolted GFRP joints at -20 °C, 20 °C and 60 °C have shown that temperature has a significant effect on the failure mode of the bolted joints. The three main failure modes are delamination, splitting and shear failure at -20 °C, 20 °C and 60 °C, respectively. The increase of temperature reduces the peak stress of the bolted GFRP joints, but increases their ductility.

(2) The simulation results have shown that E/D has little effect on the failure mode of components at -20 °C, which was mainly due to delamination. At 20 °C, with the increase of E/D, the failure mode changes from splitting to tensile failure, and at 60 °C, from shear to tensile and pressure failure. With the increase of W/D, the failure mode of the joints changes from delamination to pressure failure at -20 °C, from tensile to pressure and splitting failure at 20 °C, and from tensile failure to shear failure at 60 °C. Because the weakening effect of temperature on the strength in all directions is different, the effect of E/D and W/D on the failure models of the joints under different temperatures are not the same. It can be concluded that with the increase of E/D, a bolted GFRP joint is prone to tensile failure, and prone to pressure failure with the increase of W/D.

(3) The calibrated discrete element model is capable of simulating bolted GFRP joints, offering not only global predictions to, e.g., strength, stiffness, deformation, etc., but also simulations of delamination and transverse cracking that may occur simultaneously.

Acknowledgements

The authors are grateful for the financial support from the National Natural Science Foundation of China (Grant No. 51878518, 51738011) and the China Scholarship Council (202006270175).

References

- [1] Chambers R E. ASCE design standard for pultruded fiber-reinforced-plastic (FRP) structures[J]. *Journal of Composites for Construction*, 1997,1(1):26-38.
- [2] Ye Y Y, Liang S D, Feng P, et al. Recyclable LRS FRP composites for engineering structures: Current status and future opportunities[J]. *Composites Part B Engineering*, 2021,212(2):108689.
- [3] Yw A, Gc A, Bw B, et al. Axial compressive behavior and confinement mechanism of circular FRP-steel tubed concrete stub columns[J]. *Composite Structures*, 2020,256.
- [4] Cheng S, Feng P, Li Z, et al. Mechanical behavior of cylindrical GFRP chimney liners subjected to axial tension[J]. *Composites Part B-Engineering*, 2019,177(Nov.15):107411-1107411.
- [5] Xz A, HI B, Peng F C, et al. A review on FRP-concrete hybrid sections for bridge applications - ScienceDirect[J]. *Composite Structures*, 2020.
- [6] Anggawidjaja D, Ueda T, Dai J, et al. Deformation capacity of RC piers wrapped by new fiber-reinforced polymer with large fracture strain[J]. *Cement and Concrete Composites*, 2006,28(10):914-927.
- [7] Nhut P V, Yoresta F S, Kitane Y, et al. Improving the Shear Strength of Bolted Connections in Pultruded GFRP using Glass Fiber Sheets[J]. *Composite Structures*, 2021,255(2):112896.
- [8] Ngo T T, Pham T M, Hao H, et al. Performance of monolithic and dry joints with GFRP bolts reinforced with different fibres and GFRP bars under impact loading[J]. *Engineering Structures*, 2021,240:112341.
- [9] Itam Z, Ishak Z A M, Yusof Z M, et al. Effect on the temperature behavior of glass fiber reinforced polymer (GFRP) in various application - A review[J]. *AIP conference proceedings*, 2018,2031(1).
- [10] Robert M, Benmokrane B. Behavior of GFRP reinforcing bars subjected to extreme temperatures[J]. *Journal of Composites for Construction*, 2010,14(4):353-360.
- [11] Khaneghahi M H, Najafabadi E P, Bazli M, et al. The effect of elevated temperatures on the compressive section capacity of pultruded GFRP profiles[J]. *Construction and Building Materials*, 2020,249:118725.
- [12] Liberatore V, Ghadimi B, Rosano M, et al. Microstructural analysis of GFRP failure mechanisms after compressive load and temperature duress[J]. *Composite Structures*, 2018,203:875-885.
- [13] Hajiloo H, Green M F, Gales J. Mechanical properties of GFRP reinforcing bars at high temperatures[J]. *Construction and Building Materials*, 2018,162:142-154.
- [14] Rosa I C, Morgado T, Correia J R, et al. Shear behavior of GFRP composite materials at elevated temperature[J]. *Journal of Composites for Construction*, 2018,22(3):4018010.
- [15] Coelho A M G, Mottram J T. A review of the behaviour and analysis of bolted connections and

- joints in pultruded fibre reinforced polymers[J]. *Materials & Design*, 2015,74:86-107.
- [16] Wf A, Am A, Jp A, et al. Testing and modelling the fatigue behaviour of GFRP composites – Effect of stress level, stress concentration and frequency - ScienceDirect[J]. *Engineering Science and Technology, an International Journal*, 2020,23(5):1223-1232.
- [17] Han C L, Wang G, Li N, et al. Study on interlaminar performance of CNTs/epoxy film enhanced GFRP under low-temperature cycle[J]. *Composite Structures*, 2021,272:114191.
- [18] Borsellino C, Urso S, Alderucci T, et al. Temperature effects on failure mode of double lap glass-aluminum and glass-GFRP joints with epoxy and acrylic adhesive[J]. *International Journal of Adhesion and Adhesives*, 2021,105:102788.
- [19] Abd-El-Naby S F M, Hollaway L. The experimental behaviour of bolted joints in pultruded glass/polyester material. Part 1: Single-bolt joints[J]. *Composites*, 1993,24(7):531-538.
- [20] Abd-El-Naby S F M, Hollaway L. The experimental behaviour of bolted joints in pultruded glass/polyester material. Part 2: Two-bolt joints[J]. *Composites*, 1993,24(7):539-546.
- [21] Turvey G J. 13 - Testing of pultruded glass fibre-reinforced polymer (GFRP) composite materials and structures[M]//BAI J. *Advanced Fibre-Reinforced Polymer (FRP) Composites for Structural Applications*. Woodhead Publishing, 2013:440-508.
- [22] Turvey G J, Zhang Y. Mechanical properties of pultruded GFRP WF, channel and angle profiles for limit state/permissible stress design[J]. *Composites Part B: Engineering*, 2018,148:260-271.
- [23] Yu-qing L, Ao D, Hao-hui X, et al. Experiment on Bolted Joints of Pultruded GFRP Laminates[J]. *China Journal of Highway and Transport*, 2017,30(6):223-229.
- [24] Inbanaathan P V, Dhinesh B, Tamilarasan U, et al. Characteristics assessment on riveted, bonded and hybrid joints using GFRP composites[J]. *Materials Today: Proceedings*, 2021(11).
- [25] Yang K, Bai Y, Ding C, et al. Comparative study on mechanical performance of bolted joints with steel and fibre reinforced polymer bolts[J]. *Journal of Building Engineering*, 2021,41:102457.
- [26] Bai Y, Keller T. Delamination and kink-band failure of pultruded GFRP laminates under elevated temperatures and compression[J]. *Composite Structures*, 2011,93(2):843-849.
- [27] Cooper C, Turvey G J. Effects of joint geometry and bolt torque on the structural performance of single bolt tension joints in pultruded GRP sheet material[J]. *Composite Structures*, 1995,32(1/4):217-226.
- [28] Turvey G J, Sana A. Pultruded GFRP double-lap single-bolt tension joints – Temperature effects on mean and characteristic failure stresses and knock-down factors[J]. *Composite Structures*, 2016,153:624-631.
- [29] Turvey G J, Szulik M. Thermo-mechanically loaded glass-fibre-reinforced polymer single-bolt

- single-lap joints[J]. Proceedings of the Institution of Civil Engineers - Structures and Buildings, 2018,171(11):830-841.
- [30] Toubia E A, Alomari A, Morgan A B, et al. Influence of heat damage on the bolted double lap joint strength of pultruded E-glass/polyester composites[J]. Thin-Walled Structures, 2021,163:107764.
- [31] Feo L, Marra G, Mosallam A S. Stress analysis of multi-bolted joints for FRP pultruded composite structures[J]. Composite Structures, 2012,94(12):3769-3780.
- [32] Rosner C N, Rizkalla S H. Bolted connections for fiber reinforced composite structural members: experimental program[J]. Journal of materials in civil engineering, 1995,7(4).
- [33] Ismail Y, Sheng Y, Yang D. Discrete element modelling of unidirectional fibre reinforced polymers under transverse tension[J]. Composites Part B-Engineering, 2015,73:118-125.
- [34] Sheng Y, Yang D, Tan Y. Microstructure effects on transverse cracking in composite laminae by DEM.[J]. Composites Science and Technology, 2020,70(14):2093-2101.
- [35] Maheo L, Dau F, Andre D. A promising way to model cracks in composite using discrete element method[J]. Composites Part B-Engineering, 2015,71:193-202.
- [36] Le BD, Dau F, Charles J. Modeling damages and cracks growth in composite with a 3D discrete element method[J]. Composites Part B-Engineering, 2016,91:615-630.
- [37] Yang D, Yong S, Ye J, et al. Discrete element modeling of the microbond test of fiber reinforced composite[J]. Computational Materials Science, 2010,49(2):259.
- [38] Wan L, Yang D, Ismail Y. 3D particle models for composite laminates with anisotropic elasticity[J]. Composites Part B-Engineering, 2018,149:110-121.
- [39] Yang D, Yong S, Ye J, et al. Multi-scale modelling of damage progression in FRC laminates- Applications of DEM[J]. Composites Science and Technology, 2011,71(11):1401-1418.
- [40] Sheng Y, Yang D, Tan Y, et al. Microstructure effects on transverse cracking in composite laminae by DEM[J]. Composites Science and Technology, 2010,70(14):2093-2101.
- [41] Zha X, Wan C, Fan Y, et al. Discrete element modeling of metal skinned sandwich composite panel subjected to uniform load[J]. Computational Materials Science, 2013,69:73-80.
- [42] Yu M, Yang B, Chi Y, et al. Experimental study and DEM modelling of bolted composite lap joints subjected to tension[J]. Composites Part B: Engineering, 2020.
- [43] Turvey G J, Wang P. Environmental effects on the failure of GRP multi-bolt joints[J]. Proceedings of the Institution of Civil Engineers - Structures and Buildings, 2009,162(4):275-287.
- [44] Yan S L, Li L Y. Finite element analysis of cyclic indentation of an elastic - perfectly plastic half-space by a rigid sphere[J]. Proceedings of the Institution of Mechanical Engineers, Part C:

Journal of Mechanical Engineering Science, 2003,217(5):505-514.

- [45] Yu-qing L, Ao D, Hao-hui X, et al. Experiment on Bolted Joints of Pultruded GFRP Laminates [J]. China Journal of Highway and Transport, 2017,30(6):223-229.